Acta Pharmacologica Sinica

www.nature.com/aps

ARTICLE

A novel bispecific antibody drug conjugate targeting HER2 and HER3 with potent therapeutic efficacy against breast cancer

Hui-fang Zong[1,2], Xi Li[1], Lei Han[2], Lei Wang[1], Jun-jun Liu[1], Ya-li Yue[1], Jie Chen[2], Yong Ke[1], Hua Jiang[3], Yue-qing Xie[2,3], Bao-hong Zhang[1]✉ and Jian-wei Zhu[1,2,3]✉

Antibody drug conjugate (ADC) therapy has become one of the most promising approaches in cancer immunotherapy. Bispecific targeting could enhance the efficacy and safety of ADC by improving its specificity, affinity and internalization. In this study we constructed a HER2/HER3-targeting bispecific ADC (BsADC) and characterized its physiochemical properties, target specificity and internalization in vitro, and assessed its anti-tumor activities in breast cancer cell lines and in animal models. The HER2/HER3-targeting BsADC had a drug to antibody ratio (DAR) of 2.89, displayed a high selectivity against the target JIMT-1 breast cancer cells in vitro, as well as a slightly higher level of internalization than HER2- or HER3-monospecific ADCs. More importantly, the bispecific ADC potently inhibited the viability of MCF7, JIMT-1, BT474, BxPC-3 and SKOV-3 cancer cells in vitro. In JIMT-1 breast cancer xenograft mice, a single injection of bispecific ADC (3 mg/kg, i.v.) significantly inhibited the tumor growth with an efficacy comparable to that caused by combined injection of HER2 and HER3-monospecific ADCs (3 mg/kg for each). Our study demonstrates that the bispecific ADC concept can be applied to development of more potent new cancer therapeutics than the monospecific ADCs.

Keywords: breast cancer; bispecific antibody drug conjugate; DAR; drug distribution; target specificity

Acta Pharmacologica Sinica (2024) 45:1727–1739; https://doi.org/10.1038/s41401-024-01279-8

INTRODUCTION

Antibody-drug conjugates (ADCs) are a class of drugs that take advantage of the specificity of a monoclonal antibody (mAb) to reach target antigens expressed on cancer cells for the delivery of a potent cytotoxic payload [1, 2]. ADCs have seen a recent surge. Out of all 15 ADC drugs, 10 were approved globally after 2019 [3, 4]. Furthermore, within the 15 globally approved ADCs, three are HER2-targeted: trastuzumab emtansine (T-DM1), trastuzumab deruxtecan (T-DXd), and disitamab vedotin (RC48). In addition, there are 26 HER2-targeted ADCs in the clinical stage [5, 6]. An ADC consists of three components: antibody, linker and payload [7], and its targeting properties are mainly determined by the antibody part. In the development of therapeutic ADCs, strategies for optimizing the antibody part mainly include enhancing its specificity, affinity and internalization [7]. In the last 10 years, the rapid advancement of the bispecific antibody technology has led to the approvals of novel therapeutics, while bispecific antibody drug conjugates (BsADCs) are mainly being tested in preclinical and clinical investigations. Andreev et al. generated a BsADC targeting HER2 and PRLR antigens expressed on the breast cancer cells. They found that the BsADC killed tumor cells co-expressing HER2 and PRLR more effectively than either HER2 ADC or PRLR ADC [8]. Similar results were also observed in our group research [9]. De Goeij et al. reported an enhanced lysosomal ADC delivery via a bispecific antibody (BsAb) approach. The BsADCs targeting HER2 and CD63 not only possessed specificity on tumor-targeting but also enhanced lysosomal delivery through CD63 [10]. Two HER2-targeting BsADCs are undergoing clinical utilization: ZW49 and JSKN003 [11]. ZW49, an anti-HER2 bivalent biparatopic antibodies targeting two non-overlapping epitopes on HER2, can induce HER2 receptor clustering [12, 13]. ZW49 is currently in a Phase I clinic trial to assess the safety and tolerability in patients with locally advanced or metastatic HER2-expressing cancers (NCT03821233) [14]. In those studies, bispecific approach was adopted to enhance the cytotoxicity of ADCs.

Members of human epidermal growth factor receptors (ErbB) are potent mediators of normal cell growth and development [15, 16]. The ErbB family consists of four closely related type I trans-membrane tyrosine kinase receptors: EGFR, HER2, HER3 and HER4 [17]. Receptor dimerization (hetero- or homo-dimerization) is an essential requirement for ErbB function and the signaling activity of these receptors. The HER2–HER3 heterodimer is considered the most potent ErbB pair with respect to strength of interaction, ligand-induced tyrosine phosphorylation and downstream signaling and functions as an oncogenic unit [15]. Some researchers reported that HER3 might be a necessary partner for the oncogenic activity of HER2 in tumors over-expressing HER2 [18, 19]. In addition, co-overexpression of HER2

[1]Engineering Research Center of Cell & Therapeutic Antibody, Ministry of Education; School of Pharmacy, Shanghai Jiao Tong University, Shanghai 200240, China; [2]Jecho Institute Co., Ltd., Shanghai 200240, China and [3]Jecho Laboratories, Inc., Frederick, MD 21704, USA
Correspondence: Bao-hong Zhang (bhzhang@sjtu.edu.cn) or Jian-wei Zhu (jianweiz@sjtu.edu.cn)

Received: 16 November 2023 Accepted: 26 March 2024
Published online: 11 April 2024

and HER3 was a predictor of impaired survival of breast cancer patients [20]. Higher expression and activation of HER3 was observed in $HER2^{+}$ breast cancer cell lines with resistance to T-DM1 [21]. A number of HER3-targeting antibodies were developed for preclinical evaluation and/or clinical trials. However, to date, there is no HER3-targeting antibody approved for clinical application because of limited evidence of clinical benefit. At the same time, taking into consideration of the drug resistance of T-DM1, a BsADC targeting HER2/HER3 heterodimer would be a hopeful choice to overcome the limitation of HER3-targeting and T-DM1 therapy.

One critical aspect of ADCs and BsADCs is the number of payloads, which has a significant impact on the efficacy and pharmacokinetics of the molecules. MMAE is a synthetic derivative of dolastatin 10 that inhibits tubulin polymerization. One-third of globally approved ADC use MMAE as the payload, including brentuximab vedotin, polatuzumab vedotin, enfortumab vedotin, disitamab vedotin, tisotumab vedotin. Valine-citrulline (vc) is the most commonly used cleavable peptide linker in current clinical research [3]. One research showed that an ADC had the strongest effect of tumor growth inhibition when the linker-payload (MC-vc-PAB-MMAE) to antibody ratio was 2–4 [22]. MC-vc-PAB-MMAE based ADCs approved by FDA typically have drug-to-antibody ratio (DAR) of 3–4. Based on those success reports, we designed our BsADC with a DAR of 3.

In this study, we constructed a HER2/HER3-targeting BsADC conjugating three payloads. We characterized its target specificity and internalization ability in vitro. Furthermore, we evaluated its anti-tumor activity and therapeutic potential in breast cancers.

MATERIALS AND METHODS

Cell lines and culture conditions

The following human cell lines derive from breast tissue of female breast cancer patients: MCF7, JIMT-1 and BT474. The BxPC-3 cell line derives from pancreatic adenocarcinoma of a female patient. The SKOV3 cell line derives from ovary adenocarcinoma of a female patient. The MCF10A cell line is an epithelial cell line that was isolated from the mammary gland of a female with fibrocystic breasts. HEK 293C18 Human Embryonic Kidney cells (HEK 293E) (CRL-10852, ATCC, Manasas, VA, USA) were cultured in a growth medium consisting of a 50/50 mix of FreeStyle 293 Expression Medium (12338018, Thermo Fisher Scientific, Waltham, MA, USA) and SFM4 HEK293 medium (SH30521.02, Cytiva, Marlborough, MA, USA), containing 100 μg/mL of G418 (60220ES08, yeasen, Shanghai, China). The BT474 (TCHu143, Chinese Academy of Sciences Cell Bank, Shanghai, China) and BxPC-3 (TCHu12, Chinese Academy of Sciences Cell Bank) human cells were grown in RPMI-1640 medium (11875093, Thermo Fisher Scientific). SKOV3 (HTB-77, ATCC), MCF7 (HTB-22, ATCC) and MCF10A (CRL-10317, ATCC) cells were grown in DMEM medium (11965092, Thermo Fisher Scientific). JIMT-1 cells (ACC-589, DSMZ, Braunschweig-Süd, Germany) were grown in McCoy's 5 A medium (16600082, Thermo Fisher Scientific) containing 10% of FBS (10099141, Thermo Fisher Scientific) in the base medium. All cell lines were tested negative of mycoplasma and maintained at 37 °C in a 5% (*v*/*v*) CO_2 humidified incubator.

Generation of HER2 × HER3 BsAb by BAPTS

The bispecific antibody HER2HER3(V205C) named as 23 V was generated in house by the "Bispecific Antibody by Protein Trans-splicing (BAPTS)" platform [23–25]. The anti-HER2 antibody sequence came from trastuzumab and the anti-HER3 antibody sequence came from DL11 in the literature [26]. We mutated the amino acid residue valine to cysteine in the position 205 of the light chains to create additional conjugation sites. Transfection into HEK 293E cells was performed according to published transient transfection procedure [24, 27]. One week post-transfection the supernatant of the culture was harvested for processing while the cell viability dropped to ~50% according to the literature [28]. Expression was analyzed by SDS-PAGE and Western as needed. The fragment A (anti-HER2) and fragment B (anti-HER3) were captured by protein L affinity column (17547815, Cytiva). The 23 V BsAb was generated through BAPTS method and purified by a MMC ImpRes Multimodal Chromatography Column (29401108, Cytiva).

Generation of HER2 × HER3 BsADC by site-specific conjugation

We mutated valine to cysteine at position 205 of the light chains to create additional sites for site-specific conjugation following the literatures [29, 30]. The linker-payload MC-vc-PAB-MMAE (SET0201, Levena Biopharma, Nanjing, China) was conjugated to the antibody via the maleimidocaproyl linker through the maleimide-thiol reaction. One millimole EDTA was added into the solution containing the antibody (1 mg/mL), and then the solution was reduced by reducing agent TCEP (C4706, Sigma-Aldrich, St. Louis, MO, USA) (one hundred-fold molar excess over antibody) at 37 °C for 1 h. The reduced antibody solution was ultra-filtrated into PBS to remove excess reducing agent. To reform the interchain disulfide bonds, the reduced antibody was incubated with oxidizing agent DhAA (261556, Sigma-Aldrich) (thirty-fold molar excess over antibody) at 25 °C for 2 h. The formation of interchain disulfide bonds was confirmed by 12% non-reducing SDS-PAGE. The drug MC-vc-PAB-MMAE (twenty-fold molar excess over antibody) was dissolved into acetonitrile (ACN, 34851, Sigma-Aldrich) and incubated with the oxidized antibody at 37 °C for 30 min with PBS/ACN (*v*/*v* 80/20). The HER2-HER3(V205C)-MMAE, named 23V-MMAE BsADC, was purified by G25 desalting column (29048684, Cytiva) [31]. The coupling efficiency was calculated from the intensities of the Lcs-MMAE bands on Coomassie Brillant Blue-stained SDS-PAGE. The parental controls, anti-HER2(V205C)-MMAE (2V-MMAE) and anti-HER3(V205C)-MMAE (3V-MMAE), were also generated by the method mentioned above.

Characterization analysis of the BsADC

The BsADCs were characterized with SEC-HPLC, UV/Vis, HIC-HPLC and LC/MS. First, the purity was determined by SEC-HPLC with a TSKgel G3000SWxl, 300 Å, 7.8 cm × 300 mm (0008541, Tosoh bioscience, Tokyo, Japan) size exclusion column. The mobile phase consisted of 85% (*v*/*v*) of 0.2 M potassium phosphate, 0.25 M KCl at pH 6.95, and 15% of isopropyl alcohol. The mobile phase flow rate was 0.5 mL/min. Ten micrograms of BsAbs and BsADCs were injected for analysis, respectively.

Average DAR was characterized with UV/Vis. MC-vc-PAB-MMAE in 80/20 PBS/ACN, 23 V BsAb in PBS, 23V-MMAE BsADC in PBS were analyzed on a UV/Vis spectrophotometer UV-2700 (SHIMADZU, Tokyo, Japan). The instrument was blanked with the solvent, and measurements were performed at ambient temperature. The average DAR was derived from the ratio of the MMAE and antibody concentrations [22]. The average DAR was calculated using the formula $DAR = (\epsilon_{Ab}^{248} - R\epsilon_{Ab}^{280})/(R\epsilon_{D}^{280} - \epsilon_{D}^{248})$, where R referred to A_{248}/A_{280}. The extinction coefficients of the drug ($\in_{D}^{248} = 17759\ \mathrm{L \cdot mol^{-1} \cdot cm^{-1}}$ and $\in_{D}^{280} = 1861\ \mathrm{L \cdot mol^{-1} \cdot cm^{-1}}$) and 23 V antibody ($\in_{Ab}^{248} = 93380\ \mathrm{L \cdot mol^{-1} \cdot cm^{-1}}$ and $\in_{Ab}^{280} = 221777\ \mathrm{L \cdot mol^{-1} \cdot cm^{-1}}$) were used in the above calculation.

Drug load distributions of the BsADC were characterized with HIC-HPLC. A TSKgel Butyl-NPR, 2.5 μm, 4.6 cm × 35 mm column (0014947, Tosoh bioscience) was set to 30 °C. The mobile phase A consisted of 50 mM potassium phosphate, 2 M ammonium sulfate at pH 7.0, and the mobile phase B consisted of 75% (*v*/*v*) 50 mM potassium phosphate and 25% isopropyl alcohol. Separation was achieved with a linear gradient of 0–95% B over 25 min at a flow rate of 0.5 mL/min. Ten micrograms of the BsADC was injected for analysis.

Drug load distribution and conjugation-efficiency of the BsADC was characterized with LC/MS. First, 100 μg of the BsADC and the BsAb were deglycosylated with 1 μL PNGase F (P0704S, New England Biolab, MA, USA) at 37 °C for 24 h to remove the N-glycan. Half of deglycosylated BsADC and BsAb were reduced with 50 mM DTT (43819, Sigma-Aldrich) at 37 °C for 30 min. Approximately 1 μg of deglycosylated intact BsADC or BsAb was loaded onto an ACQUITY UPLC Protein BEH C4 Column (Waters, MA, USA) to remove the salt. A Waters Acquity Xevo G2-XS MS system was coupled with the UPLC to determine the mass of the BsAb and BsADC. The multiple charged peaks of the samples were deconvoluted using UNIFI 1.8 software (Waters). The reduced BsADC was analyzed for molecular weight changes in heavy chain and light chain.

Affinity measurement of the BsADC

Affinity of the BsADC was determined by surface plasmon resonance (Biacore 8 K, Cytiva) [32]. Human HER2-Fc (10004-H02H, Sino Biological, Beijing, China) and HER3-Fc (10201-H02H, Sino Biological) were immobilized to a CM5 chip surface (BR100399, Cytiva) using standard 1-ethyl-3 (3-dimethylaminopropyl) carbodiimide (EDC)/N-hydroxysuccinimide (NHS) amine coupling protocols. The running buffer was HBS-EP+ buffer with a flow rate of 30 μL/min. The chip surface was regenerated by 0.1 M glycine, pH 1.5. The concentration series were fit to a 1:1 binding model to determine the binding (K_a), dissociation (K_d) rate constants and the equilibrium dissociation constant (KD).

To demonstrate simultaneous antigen-antibody binding, human HER2-Fc was coupled to a CM5 sensor chip as described above. The BsADC 23V-MMAE was injected respectively for 100 s followed by a 100 s injection of HER3-Fc (at a concentration of 100 nM). The HBS-EP+ buffer was injected as a control.

Cell surface binding measured by FACS

To determine the binding effect of bispecific *vs* monospecific antibody drug conjugates on the surface of the cell lines (BT474, BxPC-3, MCF7, JIMT-1, SKOV3, MCF10A) expressing varying levels of surface HER2 and HER3, the cells in exponential growth were harvested and resuspended in FACS buffer (10^6 cells/mL in PBS + 2% FBS). 2×10^5 cells were incubated with primary antibodies at varying concentrations at 4 °C for 30 min. After 3 times washing with FACS buffer, bound antibodies were detected with FITC-labeled goat anti-human IgG (H + L) (31531, Thermo Fisher Scientific). The cells were analyzed by CytoFLEX cytometer (BECKMAN COULTER, Brea, CA, USA) for median fluorescence intensity in the FITC channel [33].

In vitro selectivity of bsAb 23 V to breast cells

Normal breast tissue MCF10A cells were stained with 2 μM PKH26 (MX4201, Shanghai Maokang Biotechnology, Shanghai, China) following the manufacturer's protocol. To evaluate the selectivity of 23 V antibody in vitro, stained cells MCF10A and unstained breast cancer cells JIMT-1 were fixed in FACS buffer, and then the bispecific antibody 23 V was added into the system incubating at 4 °C for 30 min. After washing 3 times by FACS buffer, bound antibodies were detected with FITC-labeled goat anti-human IgG (H + L). The cells were analyzed by flow cytometry for median fluorescence intensity (MFI) in the FITC and PE channels. The FITC + /PE + stands for the antibodies that could bound to MCF10A cell lines, and the FITC + /PE - refers to the antibodies that could bound to JIMT-1 cell lines. MCF10A cells were mixed with 2×10^5 JIMT-1 cells at the ratios of 1:1 and 20:1, and incubated with 23 V antibody (100 nM). Analysis was done by CytoFLEX cytometer with software CytExpert 2.3 [34].

Internalization assay

JIMT-1 cells were incubated with 23V-MMAE BsADC or 2V-MMAE (60 nM each antibody) on ice for 1 h and then washed to remove unbound antibodies. An aliquot of cells remained on ice and the rest were incubated at 37 °C for different periods of time. Cells were fixed in 2% paraformaldehyde (P0099, beyotime, Shanghai, China) for 20 min and then stained with FITC-labeled goat anti-Human IgG (H + L) secondary antibody. Stained cells were analyzed by CytoFLEX cytometer equipped with CytExpert software. Internalization of receptor-antibody complex was calculated as percent MFI loss at 37 °C relatives to that on ice after subtracting the background value of MFI derived from untreated control [35].

Cytotoxicity in vitro

BxPC-3, MCF7, JIMT-1, BT474 and SKOV3 cells were seeded into 96-well plates with 200 μL assay medium and incubated overnight at 37 °C, 5% CO_2. After 24 h, antibodies or drug conjugates (23V-MMAE, 23 V, 2V-MMAE, 3V-MMAE, 2V-MMAE + 3V-MMAE) at varying concentrations were added into the 96-well plates and incubated for 5 d. The cytotoxicity of antibodies and ADCs were determined by measuring cell viability using CCK8 kits following the manufacturer's instruction (CK04, Dojindo, Shanghai, China). The absorbance was detected using TECAN infinite 200 (Tecan Trading AG, Männedorf, Switzerland) at the wavelength of 450 nm and reference wavelength of 620 nm. Percentage of cell viability was calculated with absorbances as follows: cell viability (%) = [(sample group − blank group) / (control group-blank group)] × 100%.

Pharmacokinetics study

Ten SPF-grade BALB/c mice (20 g, male, Charles River, Beijing, China) were purchased and randomly divided into two groups. This study received ethical approval of Institutional Animal Care and Use Committee (IACUC) of Shanghai Jiao Tong University (SJTU) (No. A2018041) and was carried out in strict accordance with the guidelines established by the IACUC. The 23V-MMAE and the control 23 V antibody were injected via tail vein of the mice at a single dose of 1 mg/kg. For serum collection, blood was collected by cheek bleeding at appropriate time intervals [36]. One hundred microliter mouse blood was collected at 15 min, 6 h, day 1, 2, 4, 7, 11, 16, 21, and day 28 after administration [37]. The blood was collected in EP tubes containing anticoagulant. Serum was collected by centrifugation at 3000 × *g* at 4 °C for 10 min and preserved in −80 °C. The antibody concentrations of serum samples were quantified by ELISA. Noncompartmental pharmacokinetic parameters were calculated with WinNonlin 8.1.0 (Certara, Princeton, NJ, USA).

Growth inhibition of HER2-positive tumor xenografts in vivo

The female NOD/SCID mice (6–8 week of age; Charles River) were injected subcutaneously in the right flank with 5×10^6 JIMT-1 tumor cells (100 μL cell suspension harvested from exponentially growing cultures) [38]. Once the tumor size reached 150 mm^3, animals were randomly divided into groups of five mice. Tumor implanted mice received tail vein injections of the antibodies or ADCs. Tumor size was measured every 3 d by caliper, until tumor volume exceeded 1000 mm^3; or the animal became sick or developed tumor ulcers [39]. The tumor volume was calculated by the formula: Tumor volume = length × $width^2/2$.

To determine the BsADC's tumor growth inhibitory effect, different doses were administered to the mice bearing JIMT-1 tumor cells. We selected 0.3, 1 or 3 mg/kg, and a single injection was administered when the tumor volume reached 150 mm^3. The combo (2V-MMAE and 3V-MMAE) with the dosage at 3 mg/kg was used as a control and PBS as a placebo.

In the comparative efficacy study, the mice were injected i.v. with PBS (10 mL/kg), 2V-MMAE (10 mg/kg), 3V-MMAE (10 mg/kg), 23 V antibody (10 mg/kg) or 23V-MMAE (10 mg/kg) on d 0 and d 7. 30 mg/kg Canertinib (S1019, Selleck, Shanghai, China) was administered by oral gavage daily for 14 consecutive days as

positive control. Tumor volume was measured over the period by caliper.

These studies all have been approved by IACUC of SJTU as the research proposal No. A2018041. And we carried out in strict accordance with the guidelines established by the IACUC.

Statistical analysis

Data analysis was performed using GraphPad Prism 8.0.2 software. Where indicated, comparison between two groups was performed by two-tailed unpaired Student's *t*-test. For all experiments * is $P < 0.05$, ** is $P < 0.01$, *** is $P < 0.001$ and **** is $P < 0.0005$. Progression-free survival time was analyzed using the Kaplan–Meier method and Log-rank test.

RESULTS

Molecular design and preparation of the BsADC

Researchers reported that HER3 could be a necessary partner for the oncogenic activity of HER2 in tumors overexpressing HER2 [15]. We hypothesized that interacting with both targets HER2 and HER3 would facilitate the tumor cell-killing. The combination of anti-HER2 antibody (2 V) and anti-HER3 antibody (3 V) was evaluated in the cancer cell proliferation inhibition test and we found that the antibodies combo had a synergistic cytotoxic effect on BT474 cancer cells (Fig. 1a). Based on this result, we designed a BsADC targeting HER2/HER3 to enhance the tumor-killing activity (Fig. 1b).

We generated a BsADC with three conjugating sites by BAPTS platform technology [23, 25, 32, 39]. In the process, there would be a 5-amino acid residues "CFNAS" insertion in the hinge region after protein trans-splicing (PTS) reaction. Mass spectrometry revealed that the cysteine residues in "CFNAS" had a high oxidation efficiency (data not shown). Additionally, we mutated the amino acid valine to cysteine in the position 205 of each light chain, because the LC-V205C conjugate had a higher stability and superior in vivo efficacy compared with other mutation locus conjugates [29] (Fig. 1c).

Following the BAPTS procedure, five vectors have been constructed and co-transfected into for expression of the fragment A (HER3-3F) and fragment B (HER2-2F) (Fig. 2a) were expressed in HEK293E cells. Both fragments were purified by Capto L affinity chromatography. The fragment A was composed of three peptides, HER3 Lc(V205C), HER3 Hc(Knob) and Int^{C}-Fc(Hole) (Fig. 2b), while fragment B was composed of two peptides, HER2 V_H-C_{H1}-Int^{N} and HER2 Lc(V205C) (Fig. 2c). The fragment A and fragment B were mixed to initiate the trans-splicing reaction with the molar ratio 1:2 under reducing condition of 2 mM DTT. A new band was observed in the corresponding molecular weight (MW) on SDS-PAGE. At the meantime, the intensity of the Int^{C}-Fc (Hole) and HER2 V_H-C_{H1}-Int^{N} bands decreased (Fig. 2d). After completion of the PTS reaction, the reaction solution containing the BsAb product was dialyzed into PBS buffer and oxidized through exposure to air for 2 d. The final BsAb product was obtained after purification through a MMC ImpRes Multimodal Chromatography Column (Fig. 2e and Supplementary Fig. S1). The purity of the BsAb was about 98% by SEC-HPLC analysis (Fig. 2f), which met the requirements for conjugating drug.

The BsADC was generated by THIOMAB technology [30]. First, the cysteine and glutathione adducts of the 23 V BsAb were removed by partial reduction with TCEP followed by diafiltration. The partial reduced sample was re-oxidized by the reagent DhAA and then mixed with MC-vc-PAB-MMAE to conjugate MMAE on the BsAb, as demonstrated by nonreduced SDS-PAGE analysis (Fig. 2g). The conjugation efficiency of MMAE was evaluated preliminarily by reduced SDS-PAGE analysis. The MW of the product would increase after the MC-vc-PAB-MMAE conjugated into both light chains. The unconjugated MC-vc-PAB-MMAE was removed by G25 desalt column.

Characterization analysis of the BsADC

The BsADC was characterized by the SEC-HPLC, UV/Vis, HIC-HPLC and LC/MS methods described in the "Materials and Methods".

There were no detectable fragments but trace amount of aggregates after conjugating drugs by SEC-HPLC (Fig. 3a). The purity was about 95%.

The DAR value and drug load distribution on an ADC are very crucial to the drug efficacy and safety. The average DAR of the BsADC was determined using the UV/Vis spectrophotometric method. We confirmed primarily the maximum absorption wavelength of MC-vc-PAB-MMAE by full-wavelength scanning, and the payload showed strong absorption at 248 nm (Supplementary Fig. S2a). Because maximum absorption of an antibody at 280 nm, the DAR value can also be determined by differential absorption measurements between 248 and 280 nm. After the extinction coefficients (ε) of the BsAb and the drug MC-vc-PAB-

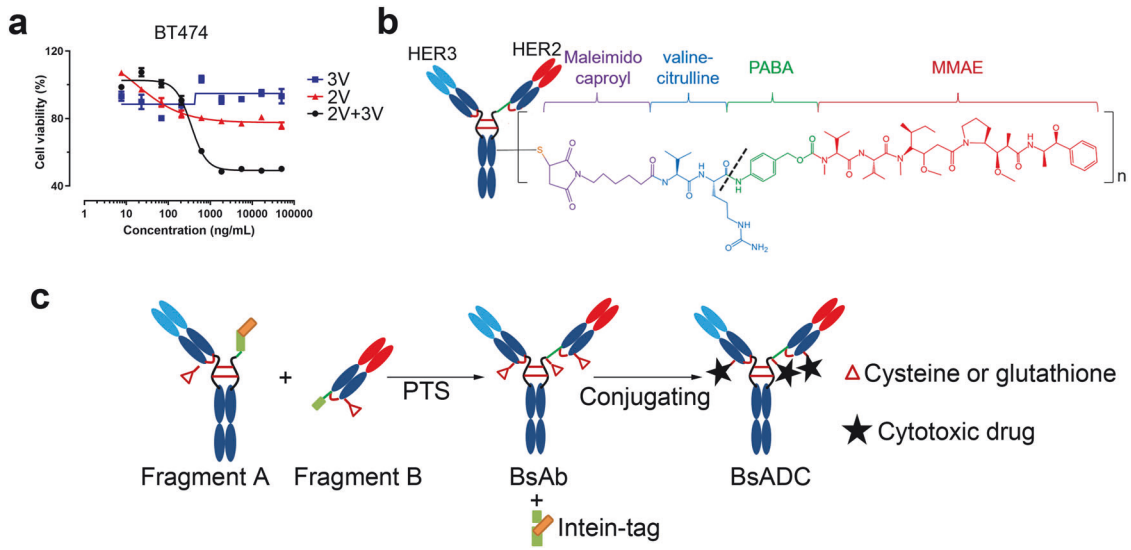

Fig. 1 Molecular design of BsADC. a The 3 V antibody functions synergistically with 2 V antibody in inhibiting BT474 cell proliferation in vitro. Representative graph shows the mean precent growth inhibition ±SEM ($n = 3$). **b** Chemical structure of BsADC. **c** Schematic representation of the split intein PTS and drug conjugation process used to generate BsADC.

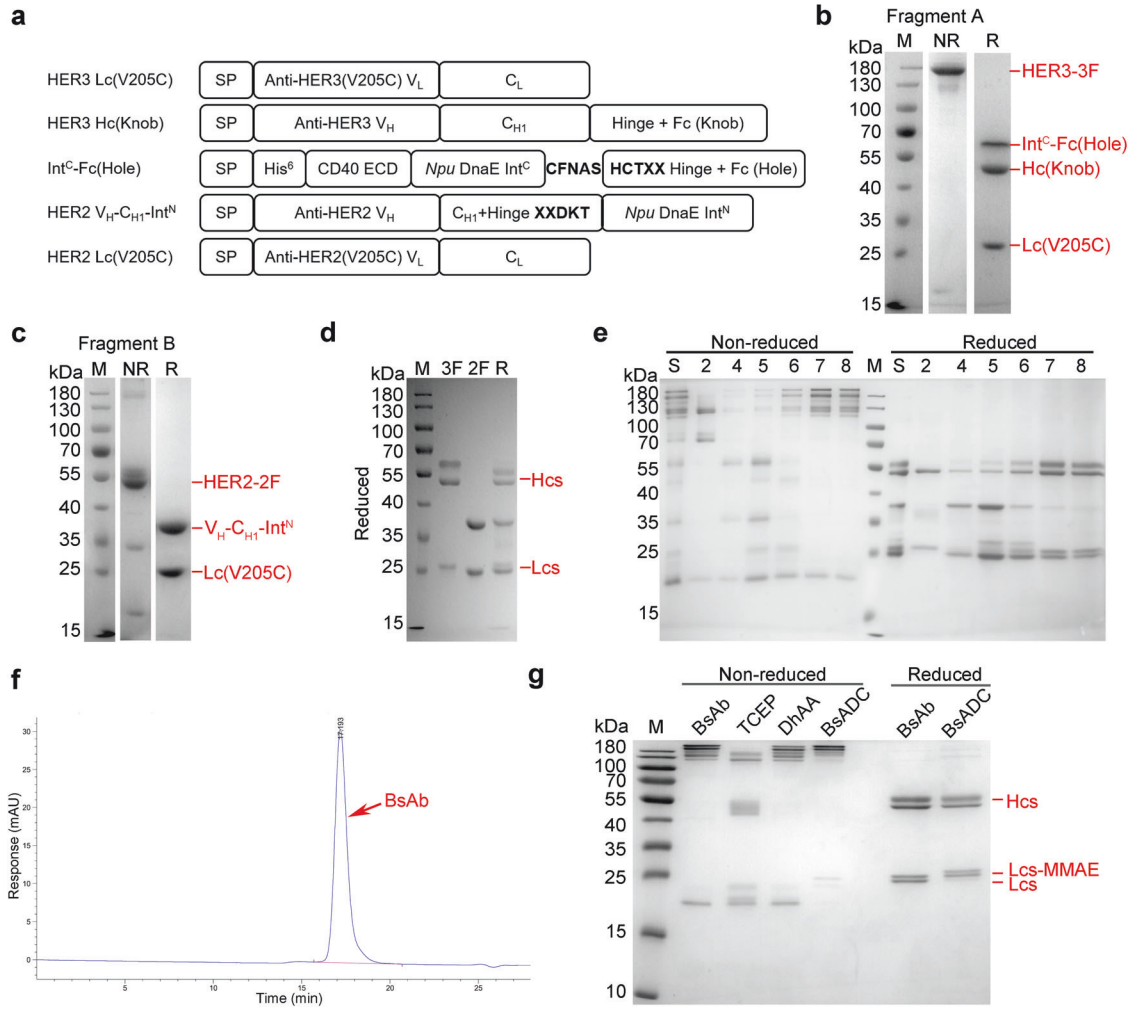

Fig. 2 Construction of BsADC. a Design of five co-transfected vectors. **b**, **c** SDS-PAGE analysis of HER3-3F (fragment A) and HER2-2F (fragment B). NR, non-reduced; R, reduced. **d** SDS-PAGE analysis of PTS reaction under reduced conditions. 3 F, HER3-3F; 2 F, HER2-2F; R, reaction sample. **e** SDS-PAGE analysis of purification products of 23 V BsAb with an MMC ImpRes Multimodal Chromatography Column. S, reaction sample; see also Supplementary Fig. S1 for the elution peak. **f** SEC-HPLC analysis of 23 V BsAb. **g** SDS-PAGE analysis of conjugating process of 23V-MMAE.

MMAE at 248 and 280 nm were determined (Supplementary Fig. S2b), we obtained the absorption spectrum of the BsADC (Supplementary Fig. S2c). The A_{248} and A_{280} of the BsADC were 0.125 and 0.192 respectively (Table 1). The average DAR value of the BsADC was 3.08 by calculation.

The HIC-HPLC method has been the gold standard for determination of DAR and drug load distribution of cysteine-conjugated ADCs. As shown in Fig. 3b, the BsADC molecules with various numbers of drug were separated, and the payload numbers of different peaks were confirmed through the absorption value of peak at UV 248 nm and 280 nm. The drug load distribution was determined through the peak area (Fig. 3c). The peak area had the highest value when the amount of payload was three. The average DAR was calculated by dividing the weighted percentage peak area by 100 and summing the divides, resulting in DAR of 2.85 for the BsADC (Table 2).

In addition, the DAR and drug load distribution of the BsADC were cross-validated by the LC/MS method. After deglycosylation by PNGaseF, the BsADC and the BsAb were analyzed at the intact protein level. The observed mass of the BsAb was 145,234 Da, which was in agreement with the theoretical mass of 145,239 Da within the range of instrument error. With BsADC, no signal was observed in the mass 145,234 Da, which demonstrated that all BsAb molecules were conjugated with various numbers of payload (Fig. 3d). The mass of first peak 146,552 Da, was 1318 Da more than the observed mass of the intact BsAb, which was consistent with the theoretical mass 1317 Da of the molecule MC-vc-PAB-MMAE. The mass intervals between adjacent peaks varied from 1317 to 1335 Da, because succinimide hydrolysis was taken place resulting in the ring-opened succinimide form of the BsADC (Supplementary Fig. S3). The corresponding payload was marked over the peak according to the MW of different components. The drug load distribution of LC/MS was determined according to the peak intensity (Fig. 3e). The average DAR was calculated by dividing the weighted percentage peak intensity by 100 and summing the quotients, resulting in DAR of 2.89 for BsADC (Table 2). The payload was mainly conjugating into the HER2 Lc(V205C), HER3 Lc(V205C) and HER2 Hc(Hole) chains as designed (Supplementary Fig. S4).

Dual binding to HER2 and HER3 antigens

To verify whether the BsAb and BsADC maintained the binding ability, we measured the binding affinity of the 23 V antibody and 23V-MMAE to HER2 and HER3 antigens by surface plasmon resonance (SPR). First, we analyzed the binding ability of the BsAb to HER2 and HER3 antigens. 2 V mAb or 3 V mAb were used as controls. Dissociation constants for 23 V BsAb to the antigens were 0.44 nM (HER2) and 13.10 nM (HER3), lower than that of the

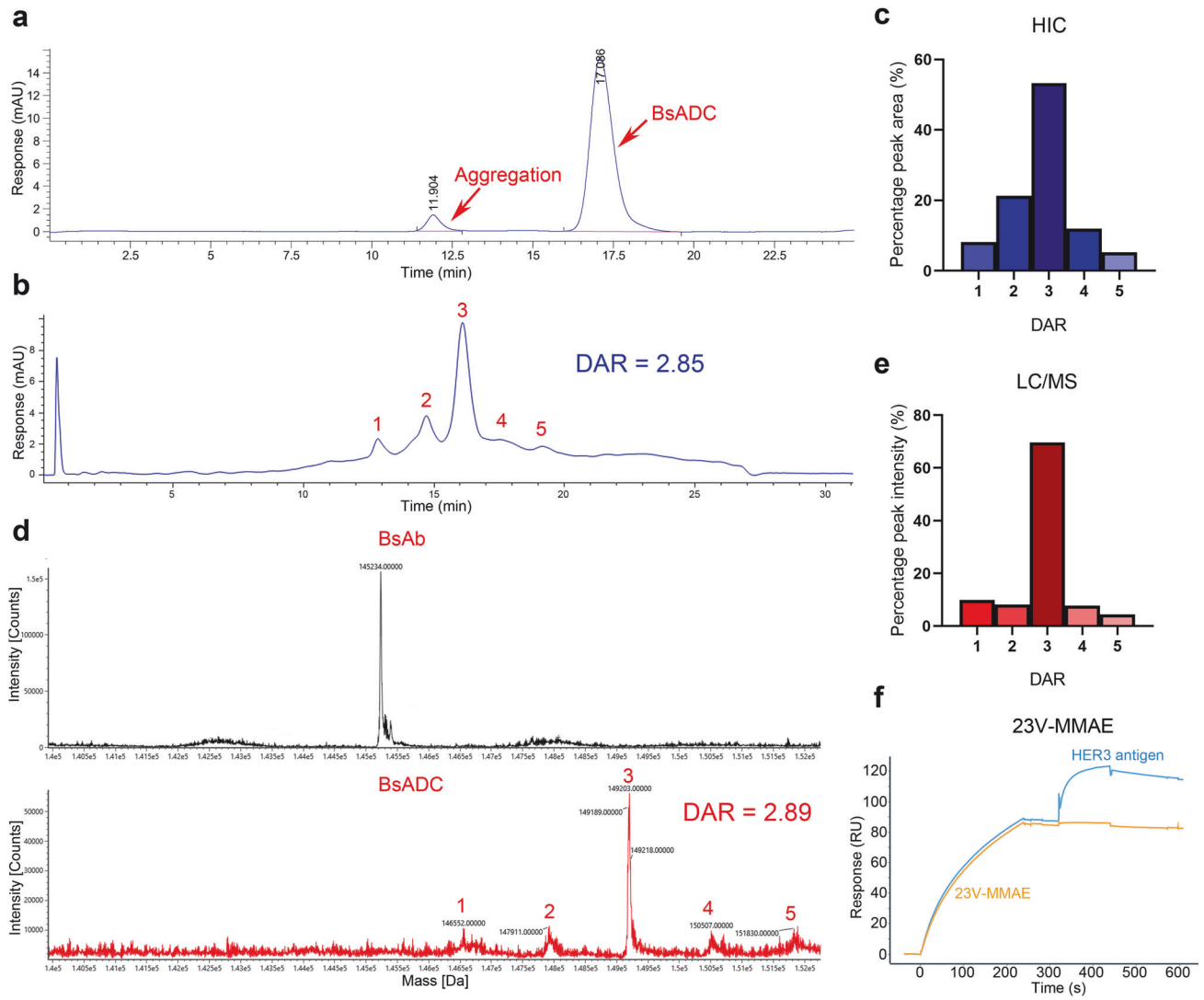

Fig. 3 Characterization of BsADC. a SEC-HPLC analysis of 23V-MMAE. **b** HIC-HPLC analysis of 23V-MMAE. The peak name refers to the number of drug load. **c** Drug load distribution of the BsADC by HIC analysis. **d** LC/MS analysis of deglycosylated intact 23 V and 23V-MMAE. The peak name refers to the number of drug load. **e** Drug load distribution of the BsADC by LC/MS analysis. The data of HIC or LC/MS column were calculated by dividing the weighted percentage peak area or peak intensity by 100. **f** The second coupling binding to HER2 and HER3 antigens of 23V-MMAE.

parental mAbs 2 V mAb 0.03 nM (HER2) and 3 V mAb 3.38 nM (HER3) (Table 3 and Supplementary Fig. S5). The differences could be caused by the monovalent structure of the BsAb. Similarly, the BsADC could bind to the antigens HER2 and HER3, but the affinity was lower than that of the parental ADCs. For HER2 antigen, the dissociation constant of 23V-MMAE was 0.54 nM vs. 0.01 nM by 2V-MMAE. Likewise, for HER3 antigen, the binding affinity of 23V-MMAE was 32.9 nM vs. 4.78 nM by 3V-MMAE (Table 3). The binding kinetics constants of the BsADC were similar to the BsAb, which indicated that the conjugation of MMAE did not alter the binding capability of the BsAb.

To determine whether the BsADC was capable of binding to HER2 and HER3 antigens simultaneously, we further performed SPR with "sandwich" binding format. Soluble HER3 antigen was injected in solution over the 23V-MMAE bound to HER2 antigen immobilized on SPR chips, using solution as a control. The BsADC showed reactive to soluble HER3 antigen, which was consistent with high-affinity antigen capture (Fig. 3f). Thus, the BsADC was confirmed to bind to HER2 and HER3 antigens simultaneously.

Cell surface binding

The efficacy of BsADCs can be influenced by the expression levels of cell surface antigens. Consequently, we chose a series of tumor cells with varying levels of surface HER2 and HER3 expression to test in vitro activity. The HER2 and HER3 surface antigen expression on tumor cells and normal breast tissue cell MCF10A were detected by flow cytometry. The expression levels of HER2 and HER3 antigens were presented in Fig. 4a. We chose the tumor cells BxPC-3 with high HER3 expression, BT474 with high HER2 expression, JIMT-1 and SKOV3 with HER2-high and balanced levels of HER2 and HER3 expression, as the target cells to detect cell surface binding of the BsADC. The cell binding ability was found to have a positive correlation with antigen expression level. Further, 23V-MMAE resulted in higher or similar levels in the MFI FITC staining compared with that of the parental ADCs (2V-MMAE or 3V-MMAE) on all cancer cell lines tested, regardless their HER2 or HER3 expression level (Fig. 4b). It was interesting that the BsADC had the best cell binding ability on JIMT-1 and SKOV3 cell lines, when the cell had expressed a balanced expression level of HER2 and HER3 antigens based on the FACS data (Fig. 4a). The

Table 1. Calculation of average DAR of the BsADC by UV/Vis measurements.

Antibody	Molar concentration (μM)	A_{248}[a]	A_{280}	ε_{248} ($M^{-1}\cdot cm^{-1}$)	ε_{280} ($M^{-1}\cdot cm^{-1}$)	DAR
MC-vc-PAB-MMAE	51.58	0.916	0.096	17759	1861	
BsAb	1.11	0.104	0.247	93380	221777	
BsADC		0.125	0.192			3.08

[a]A_{248}, Absorbance value at UV 248 nm; A_{280}, Absorbance value at UV 280 nm; ε_{248}, Extinction coefficient at UV 248 nm; ε_{280}, Extinction coefficient at UV 280 nm.

Table 2. DAR calculation of the BsADC by HIC and LC/MS analysis.

		HIC		LC/MS	
Peak name	Drug load	Percentage peak area (%)	Weighted peak area/100	Percentage peak intensity (%)	Weighted peak intensity/100
1	1	8.15	0.08	9.94	0.10
2	2	21.27	0.43	8.16	0.16
3	3	53.28	1.60	69.67	2.09
4	4	12.01	0.48	7.75	0.31
5	5	5.29	0.26	4.47	0.23
Weighted average DAR[a]			2.85		2.89

[a]The data of HIC or LC/MS weighted average DAR was calculated by summing the divides of the weighted percentage peak area or peak intensity with 100.

Table 3. The affinity measurement of the BsADC with Surface plasmon resonance (SPR).

Antigen	Antibody	K_a (1/Ms, 10^5)	K_d (1/s, 10^{-4})	KD (nM)
HuHER2	23V-MMAE	1.48	0.80	0.54
	23 V	2.25	0.99	0.44
	2V-MMAE	4.36	0.04	0.01
	2 V	4.95	0.14	0.03
HuHER3	23V-MMAE	0.46	15.00	32.90
	23 V	0.80	10.50	13.10
	3V-MMAE	1.47	7.01	4.78
	3 V	1.76	5.94	3.38

See also Supplementary Fig. S5 for SPR assay characterizing the binding kinetics of the controls.

speculated reason is that HER2 and HER3 receptors form heterodimers in tumors, allowing BsADCs to cross-link them and induce receptor clustering, potentially enhancing affinity.

In vitro selectivity

To simulate the effects of HER2 + /HER3+ normal tissue on BsAb targeting, we used fluorescein stained MCF10A normal breast epithelial cells mixed with unstained JIMT-1 cells. MCF10A and JIMT-1 cells were readily distinguishable by flow cytometry when mixed at 1:1 and 20:1 (Fig. 4c). The BsAb (100 nM) was specifically bound to JIMT-1 cells while minimally to the normal MCF10A cells at 1:1 mixed. The BsAb was detected in 99.64% of the JIMT-1 cells, while MCF10A cells failed to exhibit significant BsAb binding. However, the normal cells were predicted to be in vast excess compared with tumor cells in vivo. To mimic this situation, we incubated 23 V BsAb with JIMT-1 cells mixed with increasing numbers of MCF10A cells. It was found that even at 20:1 MCF10A to JIMT-1 ratio, the BsAb was still 99.21% on the JIMT-1 cells and only 0.32% on the MCF10A cells. The presence of the normal tissue cells had no significant interference on the ability of BsAb specifically targeting on JIMT-1 cells.

Internalization

To examine whether the BsADC could enhance internalization, JIMT-1 cells were treated with the test sample 23V-MMAE or the controls 2V-MMAE and 3V-MMAE. The cell surface levels of antibodies were measured by flow cytometry. As shown in Fig. 4d, the internalization efficiency of the cells treated with the BsADC was about 57% at 4th hour, compared with about 40% of cells treated with 2V-MMAE and 27% of cells treated with 3V-MMAE. The BsADC elicited a slightly higher level of internalization than the controls.

In vitro cytotoxicity

To evaluate tumor cell killing activity of the BsADC in vitro, a panel of human cancer cell lines expressing different levels of HER2 were selected. We treated the cancer cells with 23V-MMAE BsADC, and 23 V BsAb, using 2V-MMAE and 3V-MMAE as controls. The results reasonably showed that the cell killing activity was generally correlated to the binding of targets (Fig. 4b, e). On the cancer cell lines (JIMT-1, SKOV3 and BT474) overexpressing HER2, the killing activity of both the BsADC and 2V-MMAE was observed. Likewise, in the cancer cell line (BxPC-3) overexpressing HER3, the killing activity of both BsADC and 3V-MMAE was observed. The BsADC had cytotoxicity against JIMT-1, a cancer cell line overexpressing HER2 but no responding to T-DM1 [12, 40], and was more potent than the parental ADC controls 2V-MMAE and 3V-MMAE (EC_{50} 23V-MMAE 80.25 ng/mL vs EC_{50} 2V-MMAE 1220 ng/mL and EC_{50} 3V-MMAE 152.1 ng/mL) (Table 4). The control 23 V BsAb didn't induce significant cell death to all HER2 positive cancer cell lines including JIMT-1, SKOV3 and BT474 cell lines, suggesting that the cytotoxicity of the BsADC was mainly contributed by the conjugated payload, MMAE. We also assessed the in vitro cytotoxicity of 23V-MMAE and the combo group (2V-MMAE + 3 V-MMAE) in SKOV3 cells, showing comparable levels of cytotoxicity (Fig. 4e and Table 4). The in vitro data also suggested that the cytotoxic killing of the BsADC was correlated to the binding activity of targets.

Pharmacokinetics (PK) analysis

Linking payloads to an antibody may influence the PK profile of the ADCs. The hydrophobicity of payload such as MMAE may increase clearance and reduce ADC exposure according to literature [41]. The PK parameters of the BsAb and BsADC were evaluated in male BALB/c mice after a single tail vein i.v. administration of 1 mg/kg. The time-concentration curves of 23 V and 23V-MMAE displayed a bi-exponential disposition (Fig. 5). The PK parameters established by noncompartmental analysis were illustrated (Table 5) and showed terminal half-lives of 23 V and 23V-MMAE 4.09 and 4.65 d, respectively. The exposure of 23V-MMAE determined by the area under the curve (AUC) that was 18.01 day*μg/mL compared with that of 23 V BsAb

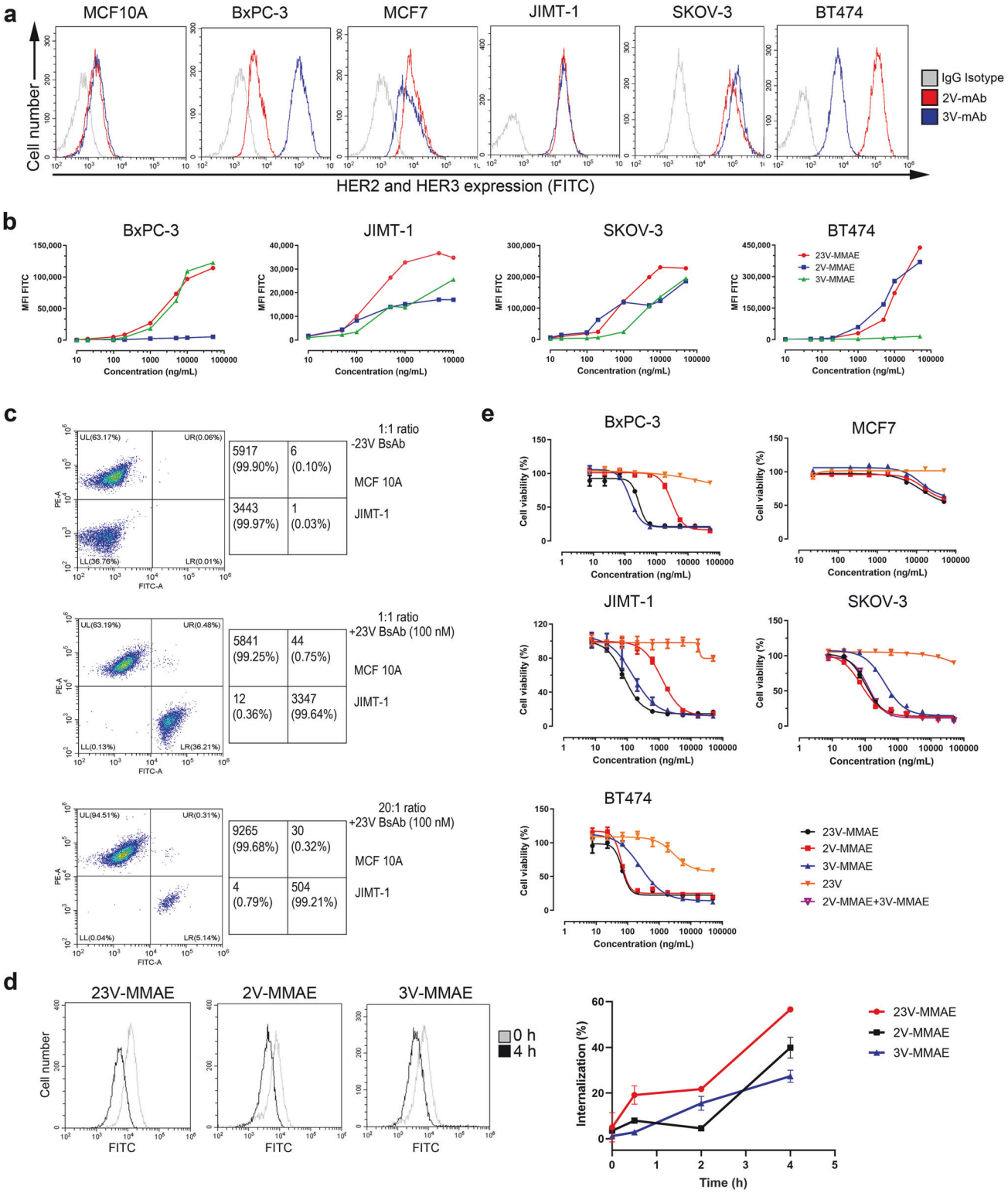

Fig. 4 Targeting selectively, internalization and in vitro cytotoxicity of BsADC. a FACS analysis of HER2 and HER3 antigen expression on different tumor cell lines and normal breast tissue cell line. **b** Titration curves of the indicated antibodies in BxPC-3, JIMT-1, SKOV-3 and BT474 cells. **c** Targeting selectively to JIMT-1 tumor cell line. Images on the left depict the raw flow cytometry data. Values on the right represent the absolute number and overall percentage of each cell type in the respective quadrants. **d** Internalization of 23V-MMAE and the controls in JIMT-1 tumor cells. **e** In vitro cytotoxicity of 23V-MMAE and the controls on tumor cell lines by CCK8 assay. Graphs are representative data derived from different cell lines showing the mean percent growth inhibition ±SEM ($n = 3$).

Table 4. EC_{50} comparison among 23V-MMAE and the controls of in vitro cytotoxicity.

	23V-MMAE		2V-MMAE		3V-MMAE		23 V		2V-MMAE + 3V-MMAE	
Cell line	EC_{50}[a]	R^2	EC_{50}	R^2	EC_{50}	R^2	EC_{50}	R^2	EC_{50}	R^2
BxPC-3	274 ± 70.5	0.96	3000 ± 410.5	0.99	145.5 ± 13.1	0.99	>40,000		ND[b]	
MCF7	13,039 ± 12.1	0.97	15,180 ± 11.5	0.95	12,865 ± 10.8	0.94	>40,000		ND	
JIMT-1	80.3 ± 15.5	0.98	1220 ± 278.2	0.98	152.1 ± 84.9	0.93	>40,000		ND	
SKOV-3	104.7 ± 13.9	0.99	77.1 ± 15.9	0.99	395.2 ± 69.9	0.99	>40,000		126.9 ± 19.5	0.99
BT474	66.9 ± 11.5	0.95	64.0 ± 8.5	0.98	258.1 ± 35.2	0.99	2938 ± 1702.5	0.88	ND	

[a]The unit of EC_{50} is ng/mL.
[b]*ND* Not detected.

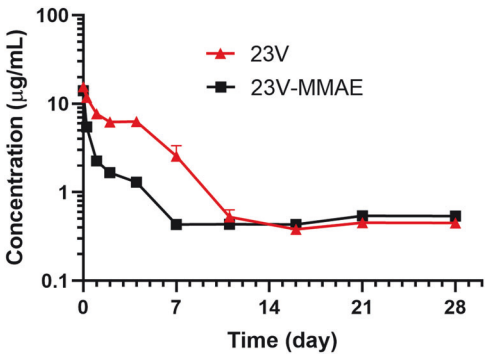

Fig. 5 Pharmacokinetics analysis of BsAb and BsADC. Antibody concentration of serum samples at different time points. BALB/c mice were injected via the tail vein with 1 mg/kg 23 V and 23V-MMAE.

Table 5. Pharmacokinetics parameters analysis of BsAb and BsADC.

	23 V	23V-MMAE
CL ($mL{\cdot}kg^{-1}{\cdot}d^{-1}$)	0.08	0.25
AUC (day*μg/mL)	56.96	18.01
C_{max} (μg/mL)	15.83	14.71
V_{ss} (mL/kg)	0.10	0.33
$t_{1/2}$ (day)	4.09	4.65

56.96 day*μg/mL. Clearance values (CL) of 23 V BsAb was 0.08 $mL{\cdot}kg^{-1}{\cdot}d^{-1}$, and it was increased to 0.25 $mL{\cdot}kg^{-1}{\cdot}d^{-1}$ for 23V-MMAE. Meanwhile, steady-state volume (V_{ss}) of 23V-MMAE was increased to 0.33 $mL{\cdot}kg^{-1}{\cdot}d^{-1}$ from 0.10 mL/kg for 23 V BsAb (Table 5). The BsADC appeared more rapid clearance than the BsAb, which was due to increasing hydrophobicity as literature reported [41–43]. The terminal half-life refers to the time required to clear one half of the drug from the plasma after reaching pseudo-equilibrium, which is determined by the terminal elimination rate [44]. Therefore, although the clearance values of the 23 V and 23V-MMAE are quite different, those two have similar terminal half-lives.

Tumor growth inhibition

To determine tumor growth inhibitory effect by the BsADC, different doses of drugs were administered to mice bearing JIMT-1 tumor cells. Twenty-five female NOD/SCID mice were injected subcutaneously with 5×10^6 JIMT-1 tumor cells/mouse and divided randomly into five groups ($n = 5$) when the tumor volume reached 150 mm^3. We first chose 0.3, 1 and 3 mg/kg as the administration dosage, and a single injection was administered when the tumor volume reached 150 mm^3 (Fig. 6a). A combo treatment (2V-MMAE and 3V-MMAE) at the dosage of 3 mg/kg was used as a control, and PBS as placebo. At low dose (0.3 and 1 mg/kg), the drug didn't show much of inhibition over the placebo group. A signification activity was demonstrated at day 24 in 3 mg/kg dose group and was comparable to the combo group (Fig. 6b). The tumor growth inhibition (TGI) of 3 mg/kg dose group and was combo group about 30%. There were no significant differences in body weight between different dose groups and combo group (Fig. 6c). Survival curves of different doses were drawn using tumor volume of 500 mm^3 as the criteria. A signification differences of survival rate between 3 mg/kg dose of the BsADC and placebo group was observed (Fig. 6d).

To improve the TGI of BsADC, we then increased the dose and dosing frequency in the subsequent in vivo experiment. We treated the JIMT-1 tumor-bearing mice with 10 mg/kg of 23 V, 2V-MMAE, 3V-MMAE and 23V-MMAE once a week for 2 weeks when the tumor volume reached 150 mm^3 (Fig. 7a), with PBS as placebo. Canertinib by oral gavage once a day for 14 consecutive days was used as a positive control. Compared with the placebo group, 23 V exhibited a slight inhibition of tumor growth and tumor weight, comparable to canertinib (Figs. 7b–d). Interestingly, 2V-MMAE also exhibited a potent inhibition of JIMT-1 tumor, a tumor resistant to T-DM1 [40].

The result also showed that 3V-MMAE had no inhibitory activity to JIMT-1 tumor, despite a decent killing effect on tumor cells in vitro (Figs. 4d and 7c). The change of body weight could partly reveal the side effect of the drugs. There were no significant differences in body weight between BsAb and ADCs, while the mice administered with canertinib showed a significant weight loss correspondent to drug filling (Fig. 7e). Survival curves of different doses were drawn using tumor volume of 500 mm^3 as the criteria (Fig. 7f).

DISCUSSION

Some BsADCs have been studied in preclinical and clinical settings. The mechanism of BsADCs to enhance cytotoxicity is likely due to the improved internalization. The cell binding of antibodies showed that 23V-MMAE BsADC had a better binding to JIMT-1 cell line compared to the controls 2V-MMAE and 3V-MMAE. The results also demonstrated that BsAb had a specific targeting to tumor cells when mixed with normal breast tissue cell MCF10A. At the same time, 23V-MMAE BsADC kept a slightly higher internalization than the control 2V-MMAE.

HER3 also plays essential roles in cancer pathogenesis and is a compelling target for cancer treatment [45]. The 3V-MMAE showed high cytotoxic activity against JIMT-1 cells in vitro. Curiously, there was no tumor growth inhibition in JIMT-1 xenograft model. There is no marketed HER3-targeting therapy and the clinical development of HER3-targeting therapeutics is

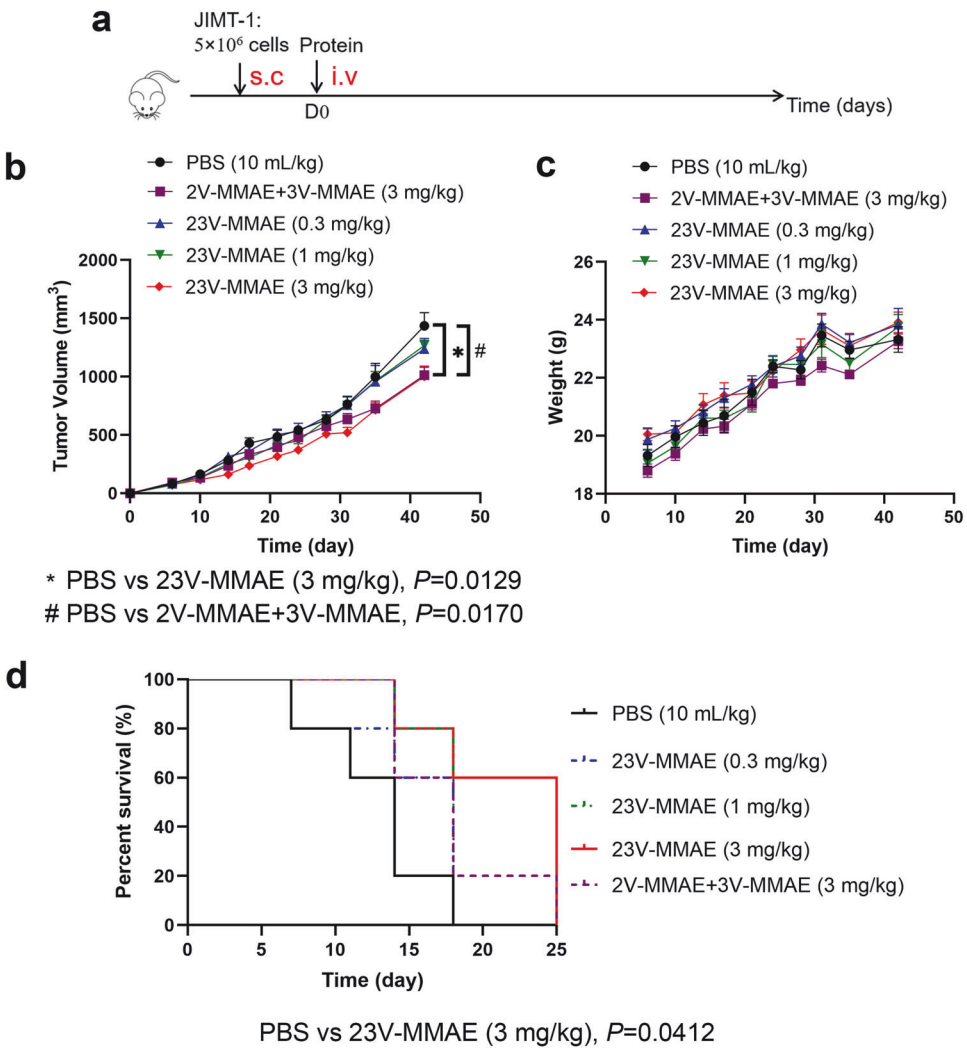

Fig. 6 Tumor growth inhibition with different dosage of BsADC and combo groups in JIMT-1 xenograft model. a Schematic schedule of tumor inoculation and treatment. Five million JIMT-1 cells/mouse were injected subcutaneously. Once tumor size reached 150 mm^3, the mice were injected i.v. with PBS (10 mL/kg) or 23V-MMAE (0.3, 1, 3 mg/kg) or the combo (2V-MMAE + 3V-MMAE) (3 mg/kg) on day 0. **b** Time course of JIMT-1 tumor-growing. Data are presented as mean ± SEM, * mean 23V-MMAE (3 mg/kg) group compared with the placebo group (*$P < 0.05$), # mean the combo group (3 mg/kg) compared with the placebo group (#$P < 0.05$). **c** Body-weight time course. **d** Changes in the percentages of surviving mice over time. Survival curves were drew using tumor volume of 500 mm^3 as the criteria.

progressing slowly due to the lack of biomarkers [46]. The tumor inhibitory effect of 2V-MMAE was similar to that of 23V-MMAE BsADC, which might be due to that the tumor-bearing JIMT-1 model was a T-DM1-resistant cell line. It was necessary to further construct a 2V-MMAE-resistant cell line for tumor growth inhibition studies in future.

There have been many reports in literature that ADCs with higher DAR values exhibit greater potency in vitro but are often inferior in vivo [22, 41, 42]. Hamblett and his colleges constructed cAC10-MMAE, which containing different drug-mAb ratios, and found that the potent activity in vitro was shown when DAR was 8 but a high therapeutic index was demonstrated when DAR was 2–4 [22]. That might be caused by the hydrophobicity of payload, lead to a pharmacokinetic penalty [41]. Our pharmacokinetic results were also similar to previous reports, the 23V-MMAE BsADC had a quick plasma clearance compared with BsAb. According to previous reports, we designed the BsADC that had about 3 drugs conjugating one BsAb. In order to reach the DAR of 3, an easily oxidized cysteine residual in the hinge region was introduced by the BAPTS bsAb production platform [24]. We also mutated the a.a. 205 in the light chain to cysteine for site specific drug conjugation, which had been reported that had a 98% conjugation efficiency and high homogeneity.

The average DAR numbers analyzed by UV/Vis, HIC, and LC/MS were slightly different. The DAR from HIC analysis was consistent with LC/MS analysis, but slightly lower than the DAR determined by UV/Vis. The change maybe caused by the aggregates in the BsADC. The drug load distribution of HIC and LC/MS showed that the majority of BsADC had three payloads, which was in line with our design. The molecular weight of MC-vc-PAB-MMAE was 1317 Da, which would change to 1335 Da after the succinimide hydrolysis resulting in ring-open form. Tumey and his colleges reported that the ring-open form linker of maleimide-based ADCs showed equivalent cytotoxicity but improved in vitro stability and PK exposure [47]. One further research direction is to promote the succinimide hydrolysis to improve the BsADC stability.

The immunoconjugates with cytotoxic agents, including ADCs, immunotoxins, or radioimmunoconjugates (RICs), are designed to enhance effectiveness of the targeted therapy. Similar to ADCs, immunotoxins are molecules containing an antibody conjugated with a peptidic cytotoxic drug via a linker [48, 49]. The specificity, affinity and internalization of antibody all need to be considered

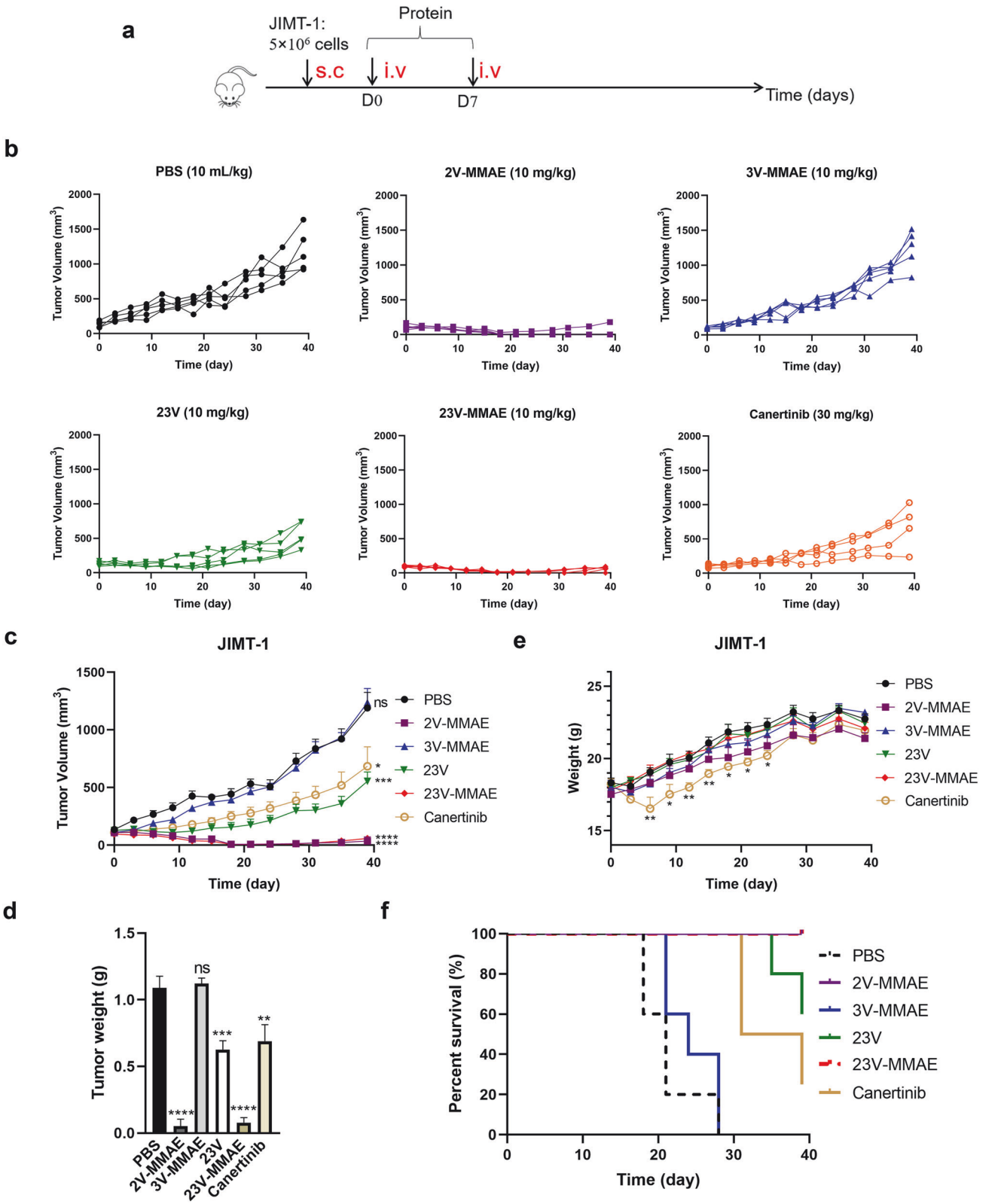

Fig. 7 Tumor growth inhibition with BsADC and the controls in JIMT-1 xenograft model. a Schematic schedule of tumor inoculation and treatment. Five million JIMT-1 cells/mouse were injected subcutaneously. Once tumor size reached 150 mm^3, thirty mice ($n = 5$) were injected i.v. with PBS (10 mL/kg), 2V-MMAE (10 mg/kg), 3V-MMAE (10 mg/kg), 23 V (10 mg/kg) or 23V-MMAE (10 mg/kg) on day 0 and 7, and administered canertinib by oral gavage once a day for 14 consecutive days. **b** JIMT-1 tumor sizes. Data were presented as measured tumor volume from different mouse. **c** JIMT-1 tumor sizes. **d** Stripping tumor weight. **e** Body-weight time course. **f** Changes in the percentages of surviving mice over time. Survival curves were drew using tumor volume of 500 mm^3 as the criteria. Data were presented as Mean ± SEM; * mean compared with the placebo group, ns means no signification, *$P < 0.05$, **$P < 0.01$, ***$P < 0.001$, ****$P < 0.0001$.

in selecting antibodies for immunotoxins and ADCs. Based on the immunotoxin researches in our laboratory [50, 51], the HER2/HER3 BsAb also could be applied to the construction of bispecific immunotoxins.

In this study, we constructed a HER2 and HER3-targeting ADC, characterized its target specificity in vitro, and evaluated its anti-tumor activity and therapeutic potential in treating breast cancers. We believe the bispecific ADC concept can be applied to the development of more potent new cancer therapeutics than the monospecific ADCs.

ACKNOWLEDGEMENTS

This work was supported by the National Natural Science Foundation of China (No. 81773621 and 82073751 to JWZ) and Shanghai Science and Technology Commission Project (No. 20S11904900 to BHZ). Authors would like to thank Lei Ma, Ai-ying Nie and Lan-kun Song at Waters Technology (Shanghai) Co. Ltd for their analytical support with mass spectrometry analysis.

AUTHOR CONTRIBUTIONS

HFZ and LH conceptualized the study. HFZ and XL designed and performed the in vitro experiments and analyzed the data. LW, JJL, YLY, JC, YK performed the in vivo experiments. HJ, YQX, BHZ and JWZ supervised the study. BHZ and JWZ provided financial support. HFZ and XL wrote the original draft. BHZ, JWZ and YQX reviewed the manuscript. All authors have read and agreed to the published version of the manuscript.

ADDITIONAL INFORMATION

Supplementary information The online version contains supplementary material available at https://doi.org/10.1038/s41401-024-01279-8.

Competing interests: The authors declare no competing interests.

REFERENCES

1. Hafeez U, Parakh S, Gan HK, Scott AM. Antibody-drug conjugates for cancer therapy. Molecules. 2020;25:4764.
2. Beck A, Goetsch L, Dumontet C, Corvaïa N. Strategies and challenges for the next generation of antibody–drug conjugates. Nat Rev Drug Discov. 2017;16:315–37.
3. Khongorzul P, Ling CJ, Khan FU, Ihsan AU, Zhang J. Antibody-drug conjugates: a comprehensive review. Mol Cancer Res. 2020;18:3–19.
4. Joubert N, Beck A, Dumontet C, Denevault-Sabourin C. Antibody-drug conjugates: the last decade. Pharmaceuticals. 2020;13:245.
5. Shi F, Liu Y, Zhou X, Shen P, Xue R, Zhang M. Disitamab vedotin: a novel antibody-drug conjugates for cancer therapy. Drug Deliv. 2022;29:1335–44.
6. Najminejad Z, Dehghani F, Mirzaei Y, Mer AH, Saghi SA, Abdolvahab MH, et al. Clinical perspective: antibody-drug conjugates for the treatment of HER2-positive breast cancer. Mol Ther. 2023;31:1874–903.
7. Chau CH, Steeg PS, Figg WD. Antibody–drug conjugates for cancer. Lancet. 2019;394:793–804.
8. Andreev J, Thambi N, Perez Bay AE, Delfino F, Martin J, Kelly MP, et al. Bispecific antibodies and antibody-drug conjugates (ADCs) bridging HER2 and prolactin receptor improve efficacy of HER2 ADCs. Mol Cancer Ther. 2017;16:681–93.
9. Zong HF, Zhang BH, Zhu J. Generating a bispecific antibody drug conjugate targeting PRLR and HER2 with improving the internalization. Pharm Fronts. 2022;04:e113–20.
10. de Goeij BE, Vink T, Ten Napel H, Breij EC, Satijn D, Wubbolts R, et al. Efficient payload delivery by a bispecific antibody-drug conjugate targeting HER2 and CD63. Mol Cancer Ther. 2016;15:2688–97.
11. Wang P, Guo K, Peng J, Sun J, Xu T. JSKN003, a novel biparatopic anti-HER2 antibody-drug conjugate, exhibits potent antitumor efficacy. Antib Ther. 2023;6:tbad014.009.
12. Li JY, Perry SR, Muniz-Medina V, Wang X, Wetzel LK, Rebelatto MC, et al. A biparatopic HER2-targeting antibody-drug conjugate induces tumor regression in primary models refractory to or ineligible for HER2-targeted therapy. Cancer Cell. 2016;29:117–29.
13. Hammood M, Craig AW, Leyton JV. Impact of endocytosis mechanisms for the receptors targeted by the currently approved antibody-drug conjugates (ADCs)-a necessity for future ADC research and development. Pharmaceuticals. 2021;14:674.
14. Pegram MD, Hamilton EP, Tan AR, Storniolo AM, Balic K, Rosenbaum AI, et al. First-in-human, phase 1 dose-escalation study of biparatopic anti-HER2 antibody-drug conjugate MEDI4276 in patients with HER2-positive advanced breast or gastric cancer. Mol Cancer Ther. 2021;20:1442–53.
15. Baselga J, Swain SM. Novel anticancer targets: revisiting ERBB2 and discovering ERBB3. Nat Rev Cancer. 2009;9:463–75.
16. Wang Z. ErbB receptors and cancer. Methods Mol Biol. 2017;1652:3–35.
17. Mitchell RA, Luwor RB, Burgess AW. Epidermal growth factor receptor: structure-function informing the design of anticancer therapeutics. Exp Cell Res. 2018;371:1–19.
18. Lee-Hoeflich ST, Crocker L, Yao E, Pham T, Munroe X, Hoeflich KP, et al. A central role for HER3 in HER2-amplified breast cancer: implications for targeted therapy. Cancer Res. 2008;68:5878–87.
19. Hsieh AC, Moasser MM. Targeting HER proteins in cancer therapy and the role of the non-target HER3. Br J Cancer. 2007;97:453–7.
20. Berghoff AS, Bartsch R, Preusser M, Ricken G, Steger GG, Bago-Horvath Z, et al. Co-overexpression of HER2/HER3 is a predictor of impaired survival in breast cancer patients. Breast. 2014;23:637–43.
21. Schwarz LJ, Hutchinson KE, Rexer BN, Estrada MV, Gonzalez Ericsson PI, Sanders ME, et al. An ERBB1-3 neutralizing antibody mixture with high activity against drug-resistant HER2^{+} breast cancers with ERBB ligand overexpression. J Natl Cancer Inst. 2017;109:djx065.
22. Hamblett KJ, Senter PD, Chace DF, Sun MM, Lenox J, Cerveny CG, et al. Effects of drug loading on the antitumor activity of a monoclonal antibody drug conjugate. Clin Cancer Res. 2004;10:7063–70.
23. Han L, Chen J, Ding K, Zong H, Xie Y, Jiang H, et al. Efficient generation of bispecific IgG antibodies by split intein mediated protein trans-splicing system. Sci Rep. 2017;7:8360.
24. Han L, Zong H, Zhou Y, Pan Z, Chen J, Ding K, et al. Naturally split intein Npu DnaE mediated rapid generation of bispecific IgG antibodies. Methods. 2019;154:32–7.
25. Zong H, Han L, Chen J, Pan Z, Wang L, Sun R, et al. Kinetics study of the natural split Npu DnaE intein in the generation of bispecific IgG antibodies. Appl Microbiol Biotechnol. 2022;106:161–71.
26. Schaefer G, Haber L, Crocker LisaM, Shia S, Shao L, Dowbenko D, et al. A two-in-one antibody against HER3 and EGFR has superior inhibitory activity compared with monospecific antibodies. Cancer Cell. 2011;20:472–86.
27. Ding K, Han L, Zong H, Chen J, Zhang B, Zhu J. Production process reproducibility and product quality consistency of transient gene expression in HEK293 cells with anti-PD1 antibody as the model protein. Appl Microbiol Biotechnol. 2017;101:1889–98.
28. Zhu J. Mammalian cell protein expression for biopharmaceutical production. Biotechnol Adv. 2012;30:1158–70.
29. Shen B-Q, Xu K, Liu L, Raab H, Bhakta S, Kenrick M, et al. Conjugation site modulates the in vivo stability and therapeutic activity of antibody-drug conjugates. Nat Biotechnol. 2012;30:184–9.
30. Junutula JR, Raab H, Clark S, Bhakta S, Leipold DD, Weir S, et al. Site-specific conjugation of a cytotoxic drug to an antibody improves the therapeutic index. Nat Biotechnol. 2008;26:925–32.
31. Francisco JA, Cerveny CG, Meyer DL, Mixan BJ, Klussman K, Chace DF, et al. cAC10-vcMMAE, an anti-CD30-monomethyl auristatin E conjugate with potent and selective antitumor activity. Blood. 2003;102:1458–65.
32. Sun R, Zhou Y, Han L, Pan Z, Chen J, Zong H, et al. A rational designed novel bispecific antibody for the treatment of GBM. Biomedicines. 2021;9:640.
33. Chen J, Pan Z, Han L, Zhou Y, Zong H, Wang L, et al. A novel bispecific antibody targeting CD3 and lewis Y with potent therapeutic efficacy against gastric cancer. Biomedicines. 2021;9:1059.
34. Robinson MK, Hodge KM, Horak E, Sundberg AL, Russeva M, Shaller CC, et al. Targeting ErbB2 and ErbB3 with a bispecific single-chain Fv enhances targeting selectivity and induces a therapeutic effect in vitro. Br J Cancer. 2008;99:1415–25.
35. Kovtun Y, Noordhuis P, Whiteman KR, Watkins K, Jones GE, Harvey L, et al. IMGN779, a novel CD33-targeting antibody-drug conjugate with DNA-alkylating activity, exhibits potent antitumor activity in models of AML. Mol Cancer Ther. 2018;17:1271–9.
36. Pan Z, Chen J, Xiao X, Xie Y, Jiang H, Zhang B, et al. Characterization of a novel bispecific antibody targeting tissue factor-positive tumors with T cell engagement. Acta Pharm Sin B. 2022;12:1928–42.
37. McDonagh CF, Turcott E, Westendorf L, Webster JB, Alley SC, Kim K, et al. Engineered antibody-drug conjugates with defined sites and stoichiometries of drug attachment. Protein Eng Des Sel. 2006;19:299–307.
38. Kang JC, Sun W, Khare P, Karimi M, Wang X, Shen Y, et al. Engineering a HER2-specific antibody–drug conjugate to increase lysosomal delivery and therapeutic efficacy. Nat Biotechnol. 2019;37:523–6.
39. Zhou Y, Zong H, Han L, Xie Y, Jiang H, Gilly J, et al. A novel bispecific antibody targeting CD3 and prolactin receptor (PRLR) against PRLR-expression breast cancer. J Exp Clin Cancer Res. 2020;39:87.
40. Barok M, Tanner M, Köninki K, Isola J. Trastuzumab-DM1 causes tumour growth inhibition by mitotic catastrophe in trastuzumab-resistant breast cancer cells in vivo. Breast Cancer Res. 2011;13:R46.

41. Lyon RP, Bovee TD, Doronina SO, Burke PJ, Hunter JH, Neff-LaFord HD, et al. Reducing hydrophobicity of homogeneous antibody-drug conjugates improves pharmacokinetics and therapeutic index. Nat Biotechnol. 2015;33:733–5.
42. Lucas AT, Price LSL, Schorzman AN, Storrie M, Piscitelli JA, Razo J, et al. Factors affecting the pharmacology of antibody-drug conjugates. Antibodies. 2018;7:10.
43. Sun X, Ponte JF, Yoder NC, Laleau R, Coccia J, Lanieri L, et al. Effects of drug-antibody ratio on pharmacokinetics, biodistribution, efficacy, and tolerability of antibody-maytansinoid conjugates. Bioconjug Chem. 2017;28:1371–81.
44. Yu R-H, Cao Y-X. A method to determine pharmacokinetic parameters based on andante constant-rate intravenous infusion. Sci Rep. 2017;7:13279.
45. Hashimoto Y, Koyama K, Kamai Y, Hirotani K, Ogitani Y, Zembutsu A, et al. A novel HER3-targeting antibody-drug conjugate, U3-1402, exhibits potent therapeutic efficacy through the delivery of cytotoxic payload by efficient internalization. Clin Cancer Res. 2019;25:7151–61.
46. Zhang N, Chang Y, Rios A, An Z. HER3/ErbB3, an emerging cancer therapeutic target. Acta Biochim Biophys Sin. 2016;48:39–48.
47. Tumey LN, Charati M, He T, Sousa E, Ma D, Han X, et al. Mild method for succinimide hydrolysis on ADCs: impact on ADC potency, stability, exposure, and efficacy. Bioconjug Chem. 2014;25:1871–80.
48. Mei X, Chen J, Wang J, Zhu J. Immunotoxins: targeted toxin delivery for cancer therapy. Pharm Fronts. 2019;1:e33–45.
49. Wu T, Zhu J. Recent development and optimization of pseudomonas aeruginosa exotoxin immunotoxins in cancer therapeutic applications. Int Immunopharmacol. 2021;96:107759.
50. Wang J, Han L, Chen J, Xie Y, Jiang H, Zhu J. Reduction of non-specific toxicity of immunotoxin by intein mediated reconstitution on target cells. Int Immunopharmacol. 2019;66:288–95.
51. Xu Y, Zhang L, Ma B, Hu L, Lu H, Dou T, et al. Intermolecular disulfide bonds between unpaired cysteines retard the C-terminal trans-cleavage of Npu DnaE. Enzym Micro Technol. 2018;118:6–12.,